frontiers in Built Environment

ORIGINAL RESEARCH
published: 22 August 2016
doi: 10.3389/fbuil.2016.00019

The 2016 Kumamoto Earthquakes: Cascading Geological Hazards and Compounding Risks

Katsuichiro Goda[1], Grace Campbell[2], Laura Hulme[2], Bashar Ismael[3], Lin Ke[4], Rebekah Marsh[5], Peter Sammonds[6], Emily So[7], Yoshihiro Okumura[8], Nozar Kishi[9], Maki Koyama[10], Saki Yotsui[8], Junji Kiyono[8], Shuanglan Wu[8] and Sean Wilkinson[11]*

[1] Department of Civil Engineering, University of Bristol, Bristol, UK, [2] Arup, London, UK, [3] School of Mechanical, Aerospace and Civil Engineering, University of Manchester, Manchester, UK, [4] Willis Towers Watson, Tokyo, Japan, [5] Mott MacDonald, Singapore City, Singapore, [6] Institute for Risk and Disaster Reduction, University College London, London, UK, [7] Department of Architecture, University of Cambridge, Cambridge, UK, [8] Graduate School of Global Environmental Studies, Kyoto University, Kyoto, Japan, [9] Karen Clark & Company, Boston, MA, USA, [10] River Basin Research Center, Gifu University, Gifu, Japan, [11] School of Civil Engineering and Geosciences, Newcastle University, Newcastle, UK

OPEN ACCESS

Edited by:
Emilio Bilotta, University of Naples Federico II, Italy

Reviewed by:
Giovanni Lanzano, Istituto Nazionale di Geofisica e Vulcanologia, Italy
Domenico Lombardi, The University of Manchester, UK

***Correspondence:**
Katsuichiro Goda
katsu.goda@bristol.ac.uk

Specialty section:
This article was submitted to Earthquake Engineering, a section of the journal Frontiers in Built Environment

Received: *11 July 2016*
Accepted: *03 August 2016*
Published: *22 August 2016*

Citation:
Goda K, Campbell G, Hulme L, Ismael B, Ke L, Marsh R, Sammonds P, So E, Okumura Y, Kishi N, Koyama M, Yotsui S, Kiyono J, Wu S and Wilkinson S (2016) The 2016 Kumamoto Earthquakes: Cascading Geological Hazards and Compounding Risks. Front. Built Environ. 2:19. doi: 10.3389/fbuil.2016.00019

A sequence of two strike-slip earthquakes occurred on April 14 and 16, 2016 in the intraplate region of Kyushu Island, Japan, apart from subduction zones, and caused significant damage and disruption to the Kumamoto region. The analyses of regional seismic catalog and available strong motion recordings reveal striking characteristics of the events, such as migrating seismicity, earthquake surface rupture, and major fore-shock-mainshock earthquake sequences. To gain valuable lessons from the events, a UK Earthquake Engineering Field Investigation Team (EEFIT) was dispatched to Kumamoto, and earthquake damage surveys were conducted to relate observed earthquake characteristics to building and infrastructure damage caused by the earthquakes. The lessons learnt from the reconnaissance mission have important implications on current seismic design practice regarding the required seismic resistance of structures under multiple shocks and the seismic design of infrastructure subject to large ground deformation. The observations also highlight the consequences of cascading geological hazards on community resilience. To share the gathered damage data widely, geo-tagged photos are organized using Google Earth and the kmz file is made publicly available.

Keywords: 2016 Kumamoto earthquake, earthquake damage survey, surface rupture, ground deformation, ground motion, building damage, infrastructure damage

INTRODUCTION

A moderate-size earthquake struck the Kumamoto region of Kyushu Island, Japan on April 14, 2016 (21:26 p.m. local time). The Japan Meteorological Agency (JMA) registered a magnitude of M_J 6.5 (moment magnitude M_w 6.1). The fault rupture originated from the northern segment of the Hinagu fault. This earthquake caused intense shaking in the eastern part of Kumamoto Prefecture, and major earthquake damage was caused in Mashiki Town near the epicenter. Subsequently, on April 16, 2016 (1:25 a.m. local time), a larger M_J 7.3 earthquake (M_w 7.1) occurred along the Futagawa fault (NE of the Hinagu fault). This earthquake caused significantly greater damage in wider areas near the fault (e.g., Mashiki Town, Nishihara Village, and Minami Aso Village). The crustal deformation

due to the mainshock was observed as ground surface rupture at many locations along the Futagawa fault (Okumura, 2016). At several places, ground deformation up to 2 m was reported (Shirahama et al., 2016). The April 14 and 16, 2016 events were of right-lateral strike-slip type occurring at shallow depths, and their focal depths were 11 and 12 km, respectively. Although the two events were originated from close but different active faults, the Government of Japan referred to these events as foreshock and mainshock, respectively; this name convention will be followed in this paper. The JMA intensity of 7 (highest intensity in the JMA intensity scale) was recorded in Mashiki Town during both the foreshock and the mainshock (i.e., double shocks). Numerous buildings had collapsed due to the double shocks. The earthquake sequence also triggered several moderate earthquakes (and some damage) at remote locations, such as Yufu City and Kokonoe Town in Oita Prefecture (about 60 km NE of Mashiki Town). Moreover, an active aftershock sequence was observed in Kumamoto. The Kumamoto earthquakes differ from so-called megathrust subduction earthquakes, such as the 2011 Great East Japan earthquake (Fraser et al., 2013; Goda et al., 2013), and have occurred in the intraplate region, similarly to the 1995 Kobe earthquake.

The earthquakes caused significant tangible and intangible loss. As of July 1, 2016, the total number of fatalities was 69 (49 deaths were directly caused by building collapses and landslides and 20 deaths were due to indirect causes), while the total number of casualties was 1,747 (Fire and Disaster Management Agency, 2016). More than 180,000 people evacuated immediately after the mainshock. The total economic loss was estimated to be 24–46 billion US dollars (Cabinet Office of Government of Japan, 2016), while the insurance loss pay-out exceeded three billion US dollars (General Insurance Association of Japan, 2016). Due to the Kumamoto earthquake sequence, 8,050 houses were destroyed, whereas 24,147 buildings suffered major damage.[1] The majority of the collapsed buildings were timber houses with heavy rooves, which were constructed according to the pre-1981 seismic design provisions (Nakashima and Chusilp, 2003). Several cultural heritages (e.g., Kumamoto Castle and Aso Shrine) were also damaged severely due to the earthquakes. The earthquakes triggered numerous landslides in the mountainous areas of the Kumamoto region, and destroyed major infrastructure and facilities. In the plain areas of Kumamoto, several sections of Kyushu Expressway (bridges and road surface cracks) were damaged due to the earthquakes, resulting in major disruption of the regional traffic network. The operation of Kyushu Shinkansen was also interrupted after the mainshock caused one Shinkansen train (traveling at 80 km/h in the south of Kumamoto railway station when the mainshock struck) to derail. Along the Aso line, which connected Kumamoto City and Aso City, a local train was derailed, whereas its railway track was destroyed by the large landslide in the Tateno district of Minami Aso Village (which also blocked the national road Route 57).

The 2016 Kumamoto disasters were caused by multiple cascading geological hazards. The primary damage was due to the intense shaking and ground deformation of the foreshock-mainshock sequence (which occurred only 28 h apart). In the near-fault region, the effects of the ground deformation were remarkable; buildings and infrastructure that were directly above the fault rupture were damaged severely. The secondary damage was caused by landslides and other ground failures, including liquefaction, settlement, and lateral spreading along rivers and coastal areas. The earthquake damage was widespread over the rural areas of Kumamoto Prefecture. In particular, simultaneous damage/destruction to multiple key infrastructures, such as Aso bridge, Oogiribata bridge, Choyo bridge, and Tawarayama tunnel, disconnected main access routes (e.g., Route 57 and Road 28) between areas inside and outside Aso Caldera. As of June 2016, major detours were required to visit places inside Aso Caldera from the Kumamoto city center. In particular, this caused significant difficulty and stress to evacuees and recovery activities in Minami Aso Village, where devastating damage was observed.

This paper presents a summary of the rupture and ground motion characteristics of the 2016 Kumamoto earthquake sequence, and relates them to the observed earthquake damage during the sequence. The damage observations were made during the UK Earthquake Engineering Field Investigation Team (EEFIT) mission,[2] which was conducted between May 22, 2016 and May 26, 2016. To share the gathered damage data widely, geo-tagged photos are organized using Google Earth and the kmz file is made publicly available as supplementary information to this paper. The investigations highlight considerable earthquake shaking and deformation demand in the near-fault region, and provide useful insights for enhancing community resilience against major earthquake disasters. First, key features of the 2016 Kumamoto earthquake sequence are discussed by looking into geological conditions and active fault zones near the Futagawa and Hinagu faults. The spatiotemporal process of the foreshock–mainshock–aftershock sequence is characterized through observed seismic activities and seismological models, such as the Gutenberg–Richter relationship and the modified Omori's law. The available finite-fault model for the mainshock is used to estimate the ground deformation in the near-fault region. Second, ground motion characteristics of the foreshock and mainshock are studied in detail by analyzing ground motion records from the K-NET and KiK-net.[3] Especially, orientations of the deformation and intense ground shaking are compared with those of the damaged buildings in the near-fault region. Third, earthquake damage survey results and observations during the EEFIT mission are discussed to relate observed damage characteristics and patterns to recorded ground motions and ground deformation. Finally, aspects of the cascading geological hazards and their consequences on infrastructure and community resilience are discussed. Useful conclusions are drawn from the investigations to promote effective risk management of compounding earthquake disasters in the future.

[1] http://www.fdma.go.jp/bn/2016/

[2] https://www.istructe.org/resources-centre/technical-topic-areas/eefit

[3] http://www.kyoshin.bosai.go.jp/

2016 KUMAMOTO EARTHQUAKE SEQUENCE

Futagawa–Hinagu Faults

The Futagawa fault stretches from the outskirt of Aso Caldera to Uto Peninsula (Headquarters for Earthquake Research Promotion, 2016). Its orientation is ENE-WSW. The total length of the fault exceeds 64 km, consisting of three segments: Futagawa segment (circa 29 km), Uto segment (circa 20 km), and Uto Peninsula segment (circa 27 km). On the other hand, the Hinagu fault touches on the Futagawa fault in the north (near Mashiki Town) and extends to Yatsushiro Sea in the south (NE–SW orientation). The total length exceeds 80 km, consisting of three segments: Takano-Shirahata segment (circa 16 km), Hinagu segment (circa 40 km), and Yatsushiro Sea segment (circa 30 km). Both Futagawa and Takano-Shirahata segments are of right-lateral strike-slip type. Historically, there have been damaging earthquakes in the Kumamoto region. For instance, the M_w 6.3 1889 earthquake caused notable damage in Kumamoto City (20 deaths, 54 injuries, and 239 house collapses; Headquarters for Earthquake Research Promotion, 2016). However, the damage severity and earthquake impact of the 2016 sequence are far greater than these relatively recent damaging earthquakes in Kumamoto.

Figure 1A shows the Futagawa fault segment and the Hinagu (Takano-Shirahata) fault segment, based on the active fault database by the National Institute of Advanced Industrial Science and Technology (2016). In **Figure 1A**, epicentral locations of the April 14, 2016 foreshock and the April 16, 2016 mainshock are shown based on the unified JMA catalog, available from Hi-net.[4] In addition, locations of Kumamoto City, Mashiki Town, Nishihara Village, and Minami Aso Village are indicated with square symbols. The thin grey lines represent political boundaries of the municipalities in the Kumamoto region. **Figure 1B** shows an elevation map of the Kumamoto region based on the GDEM database.[5] The NE end of the Futagawa segment lies at the opening of the walls of Aso Caldera.

The most recent seismic hazard assessment by the Headquarters for Earthquake Research Promotion (2016) has taken into account rupture scenarios from the Futagawa and Hinagu faults. In the assessment, a scenario magnitude for the Futagawa segment is set to M_w 7.0 with occurrence probability of less than 1% in 30 years, noting that there is a possibility that all three segments of the Futagawa fault rupture simultaneously (in this case, the magnitude is estimated to be in the range of M_w 7.5–7.8). On the other hand, a scenario magnitude for the Hinagu (Takano-Shirahata) segment is considered to be M_w 6.8 with unknown occurrence probability. Similarly to the Futagawa fault, there is a possibility that all three segments of the Hinagu fault could rupture simultaneously, resulting in an M_w 7.7–8.0 earthquake. Moreover, because of the proximity of the Futagawa segment and the Takano-Shirahata segment, both faults might rupture simultaneously, potentially leading to an M_w 7.8–8.2 event. Importantly, during the 2016 Kumamoto earthquake sequence, numerous events occurred initially along the Takano-Shirahata segment (e.g., 14 April foreshock), and then along the Futagawa segment (e.g., 16 April mainshock).

The preceding hazard information (i.e., earthquake rupture potential of the Hinagu and Futagawa fault systems) has been utilized by the Headquarters for Earthquake Research Promotion in developing a wide range of probabilistic seismic hazard maps in Japan.[6] One type of seismic hazard maps display the probability of experiencing a certain shaking intensity in a 30-year period by

[4]http://www.hinet.bosai.go.jp/

[5]https://asterweb.jpl.nasa.gov/gdem.asp

[6]http://www.j-shis.bosai.go.jp/en/

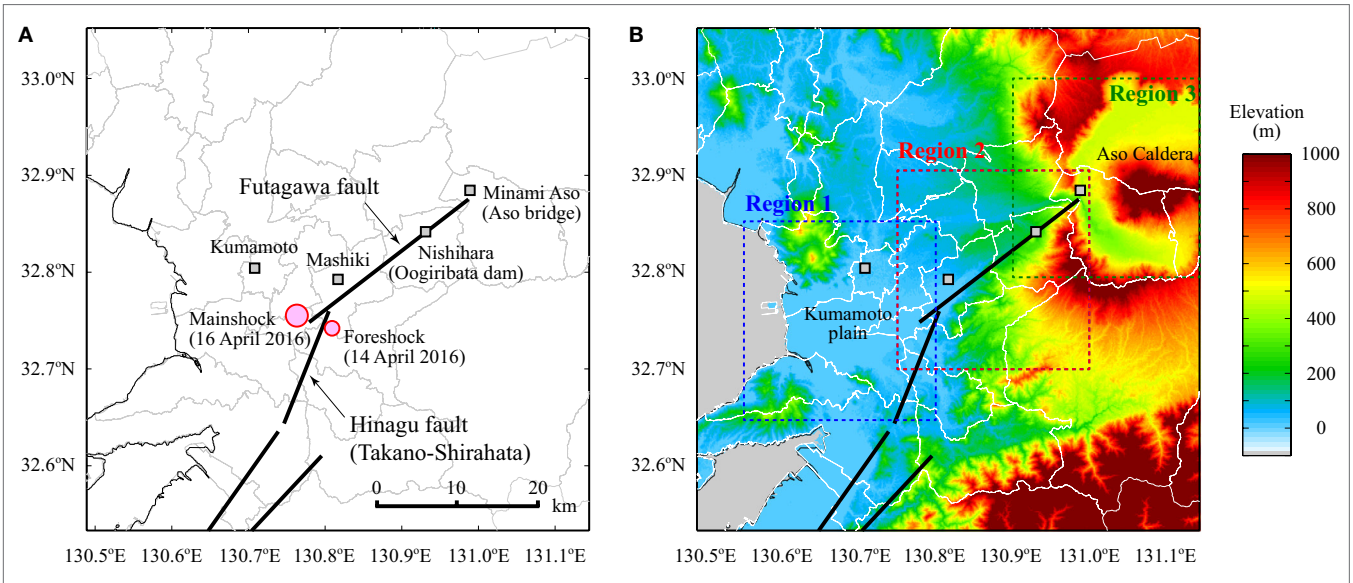

FIGURE 1 | **(A)** Locations of the Futagawa–Hinagu faults. **(B)** Elevation map of the Kumamoto region.

taking into account all possible seismic sources surrounding a site of interest. Another type is the scenario-based shaking map that is generated by the Green's function method using the characterized source model (Irikura and Miyake, 2011).

Seismic Activities

A prolific sequence of earthquakes was observed in the Kumamoto region, after the triggering foreshock event of April 14, 2016. **Figure 2A** shows the temporal variation of earthquakes having $M_J > 3$ over a period between April 13, 2016 and April 18, 2016, while **Figures 2B–F** show the spatial distribution of earthquakes occurring in different time periods. The earthquake data were based on the JMA catalog. The M_J 6.5 foreshock induced an active sequence of dependent events (including a M_J 6.4 event on April 15, 2016). From the spatial distribution of the events that occurred between the foreshock and the mainshock (**Figure 2D**), it can be observed that the triggered events by the foreshock were clustered along the Hinagu fault. Subsequently, the mainshock occurred on the southern tip of the Futagawa fault, and triggered an even more active subsequence of aftershocks (**Figures 2E,F**). The aftershock sequence was not only concentrated along the Futagawa–Hinagu faults but also in the Aso region (NE of the Futagawa fault). The migration of seismic activities over relatively wide spatial areas is a notable feature of the 2016 Kumamoto earthquake sequence.

Using the observed earthquake data in the Kumamoto region, statistical analysis of aftershocks is carried out by applying the Gutenberg–Richter law (i.e., frequency-magnitude characteristics of an aftershock sequence) and the modified Omori law (temporal decay of an aftershock occurrence rate; Guo and Ogata, 1997). It is considered that the JMA catalog is complete above M_J 3.5. In fitting these seismological models, the entire catalog is divided into two parts: events that occurred between the foreshock and the mainshock (72 earthquakes), and events that occurred after the mainshock (248 earthquakes). The results are shown in **Figure 3**. Due to the longer period and the larger triggering event, the number of events in the mainshock-aftershock sequence is greater than that of the foreshock-mainshock sequence. The b-value of the mainshock–aftershock sequence is steeper and has a value close to a typical b-value of 1.0 (Guo and Ogata, 1997). For the modified Omori law, the temporal decay parameter (p-value) for both datasets is estimated as 1.0, which is broadly consistent with the past studies of aftershock statistics (Guo and Ogata, 1997).

Finite-Fault Models and Estimated Ground Deformation

Finite-fault source models, which are determined through source inversion analysis, provide plausible images of earthquake rupture processes by achieving the consistency between observed data and geophysical model predictions (e.g., geodetic, teleseismic, and strong motion). After the Kumamoto foreshock and mainshock, several finite-fault models have been developed and were made available publicly. For example, the Geospatial Institute of Japan (GSI) (2016) developed finite-fault models for the Kumamoto foreshock and mainshock based on GEONET GPS observations. The finite-fault models for the foreshock and mainshock are shown in **Figure 4A**. The geometry is consistent with the fault strike by the National Institute of Advanced Industrial Science and Technology (**Figure 1A**). The estimated slip values for the foreshock and mainshock are 0.62 and 3.50 m, respectively (assumed to be uniform across the fault plane).

For the mainshock, at the Kumamoto GEONET station (32.8421°N, 130.7648°E), 0.75 m horizontal deformation in the ENE direction and 0.20 m downward deformation were recorded, while at the Choyo GEONET station (32.8707°N, 130.9962°E), 0.97 m horizontal deformation in the SW direction and 0.23 m upward deformation were recorded. These observations serve as important constraints in developing finite-fault models for the mainshock, indicating that the fault strike (approximately SW to WSW) should lie between the Kumamoto and Choyo stations.

Using the geometry and slip distribution of a finite-fault model, elastic deformation due to an earthquake can be calculated using Okada (1985) equations. The analytical formulae allow the estimation of NS, EW, and UD components of ground surface deformation. The results of the calculated elastic deformation profiles based on the GSI finite-fault model for the mainshock are shown in **Figures 4B–D**. The results at the GPS stations presented in **Table 1** and show good agreement, demonstrating that the GSI models are particularly useful for estimating permanent deformation at unmonitored locations due to the earthquake.

STRONG GROUND MOTION CHARACTERISTICS

In Japan, national strong motion networks, K-NET and KiK-net, were established after the 1995 Kobe earthquake, and currently more than 1,700 stations are operational. For the 2016 Kumamoto earthquakes, an extensive set of ground motion data is available. In this section, characteristics of observed ground motions in the Kumamoto region are investigated by focusing on: (i) strong motion characteristics in the near-fault region, (ii) regional ground motion characteristics and orientations of the major response axis with respect to the fault strike direction, (iii) comparison of observed ground motion recordings with an existing ground motion prediction equation (GMPE), and (iv) estimation of ground motion parameters at unobserved locations. For these purposes, available ground motion data for 20 seismic events that occurred in April 2016 ($M_J \geq 4.3$) are downloaded from the K-NET and KiK-net (in total, 6,177 records, including borehole recording data for the KiK-net; each record has three components), and are processed uniformly to compute acceleration and velocity waveforms as well as various ground motion parameters [peak ground acceleration (PGA) and 5%-damped spectral acceleration (SA)]. For the record processing, a standard procedure (e.g., tapering, zero-padding, and band-pass filtering) suggested by Boore (2005) is implemented.

Strong Motion Characteristics in the Near-fault Region

Ground motion data recorded at KMMH16 (Mashiki; 32.7967°N, 130.8199°E) are analyzed in detail, noting that the earthquake damage surveys were conducted near this station during the EEFIT mission. The KMMH16 station belongs to

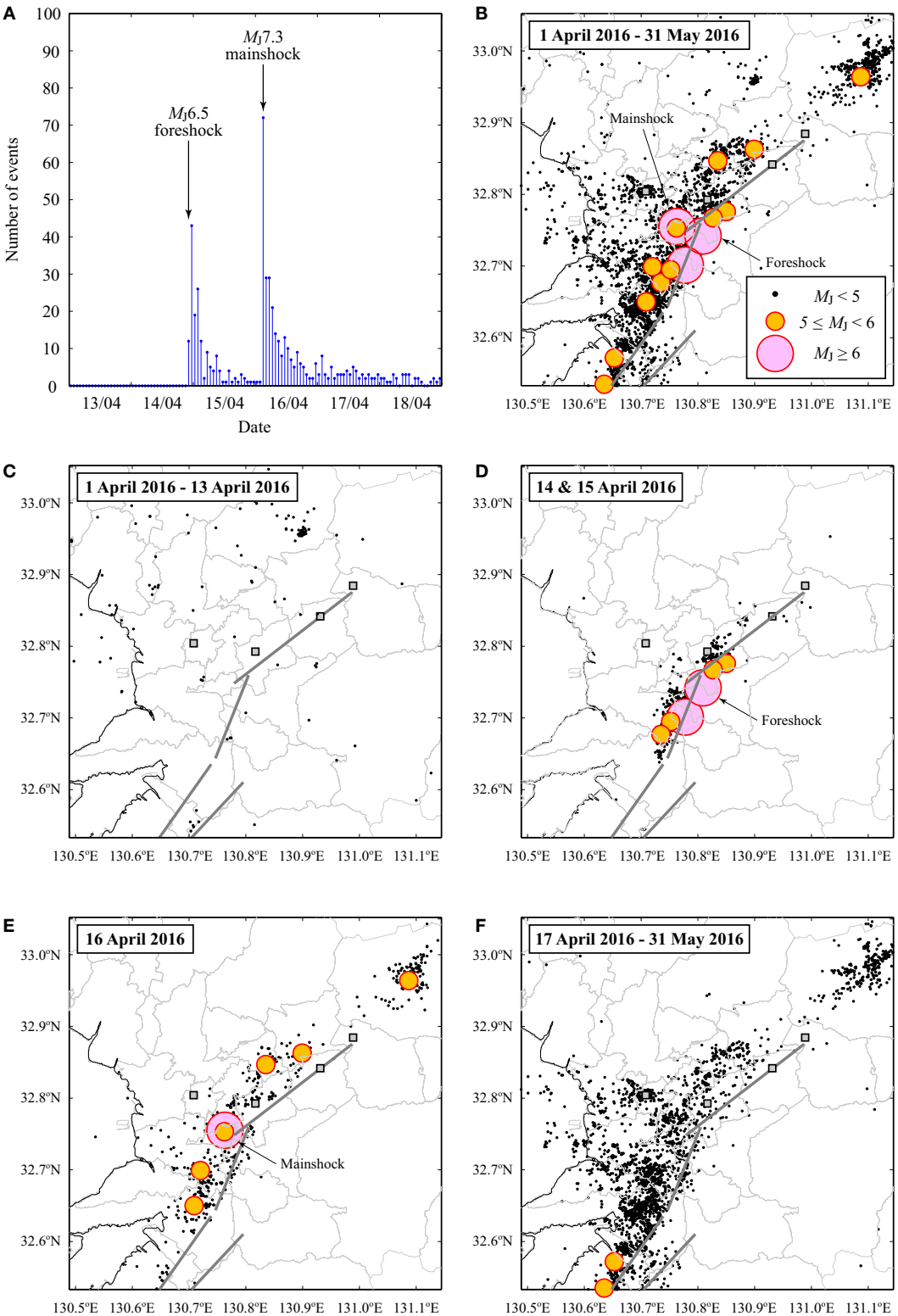

FIGURE 2 | **(A)** Number of earthquakes with $M_J > 3$ that occurred in the Kumamoto region during April 1, 2016 to May 31, 2016. Spatial distribution of earthquakes in the Kumamoto region: **(B)** April 1, 2016 to May 31, 2016, **(C)** April 1, 2016 to April 13, 2016, **(D)** April 14 and 15, 2016, **(E)** April 16, 2016, and **(F)** April 17, 2016 to May 31, 2016.

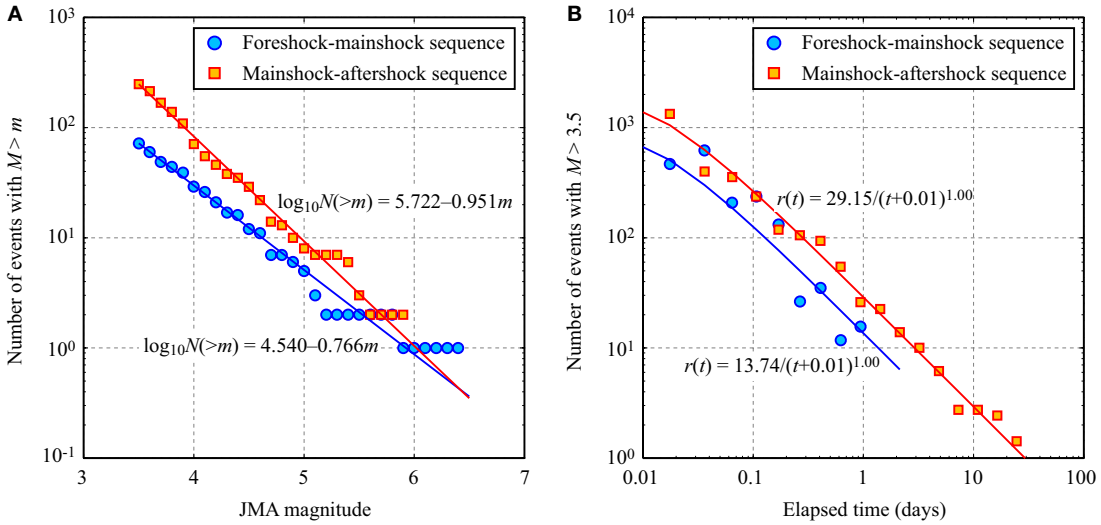

FIGURE 3 | Characteristics of foreshock-mainshock and mainshock-aftershock sequences: (A) Gutenberg–Richter models and (B) modified Omori models.

the KiK-net, and thus two sets of three component recordings at the ground surface and in borehole are available, enabling site amplification effects to be investigated. Another important aspect of the selected records is that KMMH16 is in the hanging wall region of the mainshock (i.e., within a projected fault plane on the ground surface), and thus intense ground shaking was observed during the mainshock. Moreover, at KMMH16, strong shaking due to the foreshock preceded the mainshock, resulting in double-shock ground motions (Kojima and Takewaki, 2016).

Figure 5 shows observed acceleration as well as velocity time-histories (three components) at KMMH16 for the foreshock and mainshock. The blue curves are for the ground surface recordings, whereas the red curves are for the borehole recordings. The significant amplification as well as different dominant frequency content of the ground motions can be observed by comparing the blue and red curves. Another notable observation is that for the velocity time-histories of the mainshock (i.e., **Figure 5D**), relatively large velocity waves are present at both ground surface and borehole (particularly for vertical motions). This indicates that site amplification for short-period components is significantly influenced by near-surface soil characteristics, while that for longer period components is more coherent at ground surface and borehole. The latter may also be attributed to the ground surface rupture near the Mashiki areas.

To examine the spectral content of the observed ground motions at KMMH16, 5%-damped response spectra for the foreshock and mainshock are calculated and shown in **Figure 6**. The results for the ground surface motions are presented with solid lines, while those for the borehole motions are shown with broken lines. The comparison of the response spectra indicates: (i) amplitudes of the response spectra are large, exceeding 1 g up to a period of about 1 s for the foreshock and about 2 s for the mainshock; (ii) generally site amplification is significant for all three components; (iii) horizontal motions are amplified in a period range between 0 s (i.e., PGA) and about 2–3 s, while vertical motions are significantly amplified at vibration periods less than 0.5 s.

At the KMMH16 station, relatively soft soil layers exist in the top 15 m (shear wave velocity less than 250 m/s), underlain by firm rock layers (**Figure 7A**). The borehole recording is installed at a depth of 255 m (ground surface is at 55 m altitude). Hence, major site amplification is anticipated between ground surface and borehole at this site because of high contrast of the shear wave velocities. The average shear wave velocity in the top 30 m of the soil (i.e., V_{s30}) is calculated as 280 m/s (i.e., NEHRP site class D). To investigate the site amplification at KMMH16 in detail, the borehole-to-surface ratios of Fourier amplitude spectra (Ghofrani et al., 2013) are computed for all 20 earthquakes that are analyzed as part of this study. The results are shown in **Figures 7B–D**; the borehole-to-surface spectral ratio curves are categorized into four groups, i.e., foreshock, events that occurred between the foreshock and the mainshock, mainshock, and events that occurred after the mainshock. The division of the datasets is intended for studying the temporal changes of the site response related to soil non-linearity during the Kumamoto foreshock–mainshock–aftershock sequence [e.g., Sawazaki et al. (2009) and Wu et al. (2009)]. The results indicate that the site amplification is period dependent; the horizontal ground motions are amplified significantly (by a factor of 5 or more) in the period range between 0.3 and 2.0 s, while the vertical ground motions are mainly amplified in the periods less than 0.5 s. For the horizontal components (**Figures 7B,C**), period shifts of the surface-to-borehole spectral ratios can be observed for the foreshock and mainshock in comparison with the majority of other smaller earthquakes

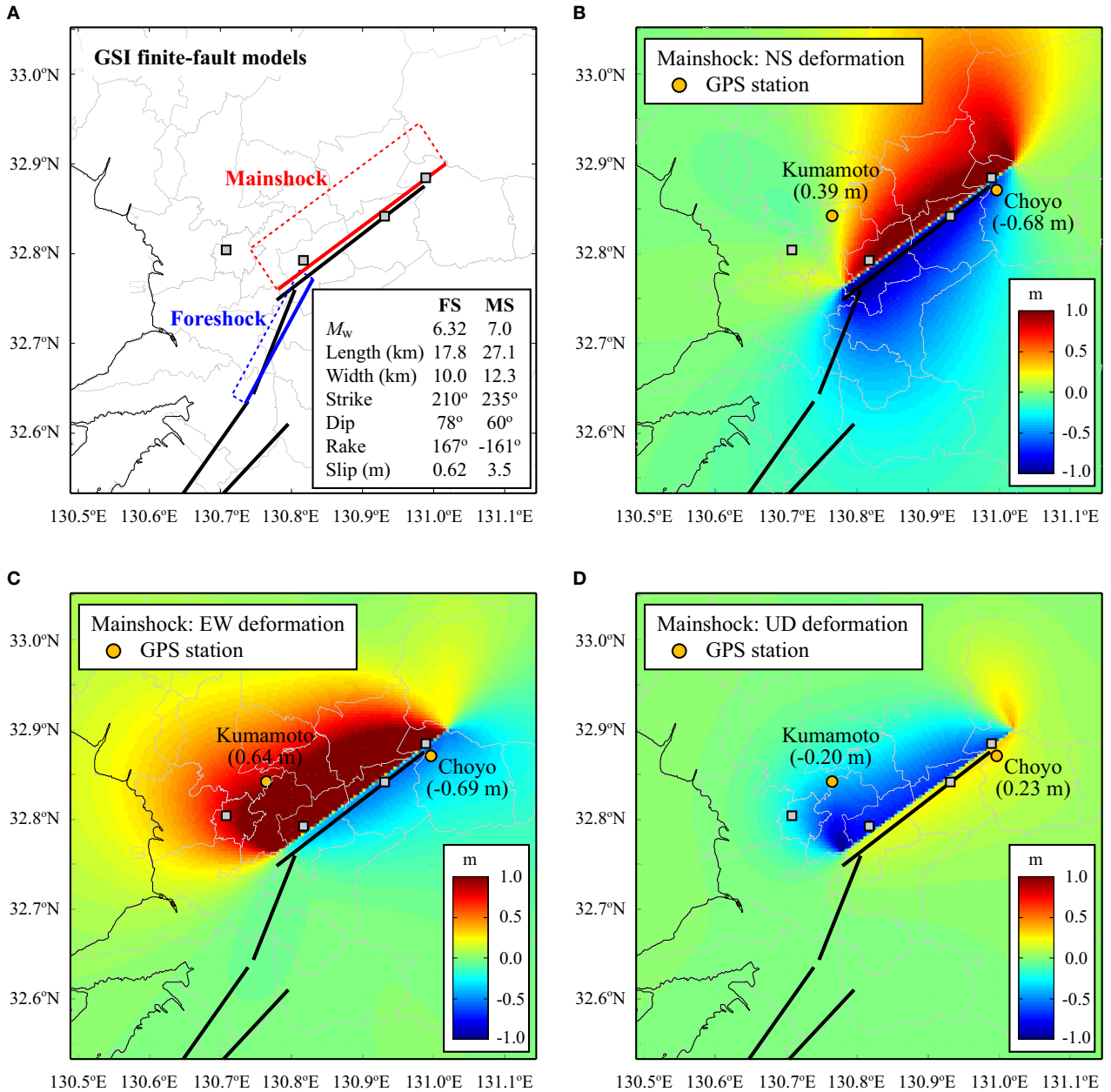

FIGURE 4 | **(A)** Finite-fault models by Geospatial Institute of Japan (GSI) (2016) for the foreshock and mainshock. Estimated elastic deformation profiles based on the GSI finite-fault model for the mainshock: **(B)** NS deformation, **(C)** EW deformation, and **(D)** UD deformation.

TABLE 1 | Comparison of the observed and estimated ground deformations at the Kumamoto and Choyo GPS stations for the mainshock.

GPS station	Observed deformations [NS, EW, UD (m)]	Estimated deformations [NS, EW, UD (m)]
Kumamoto	[0.39, 0.64, −0.20]	[0.0, 0.85, −0.30]
Choyo	[−0.68, −0.69, 0.23]	[−0.57, −0.50, 0.25]

(i.e., dominant peaks of the spectral ratios at 0.2–0.4 s are significantly reduced). For the vertical component (**Figure 7D**), very consistent site amplification is observed at periods less than 1.0 s, while the surface-to-borehole spectral ratios become more variable at longer periods. These observations are a strong argument for making more detailed investigations of the site amplification and the non-linear site response.

Regional Ground Motion Characteristics

It is interesting to investigate the amplitude and orientation of ground motion parameters with respect to the fault strike (Watson-Lamprey and Boore, 2007). For this purpose, the analyses of ground motion records are extended to other K-NET

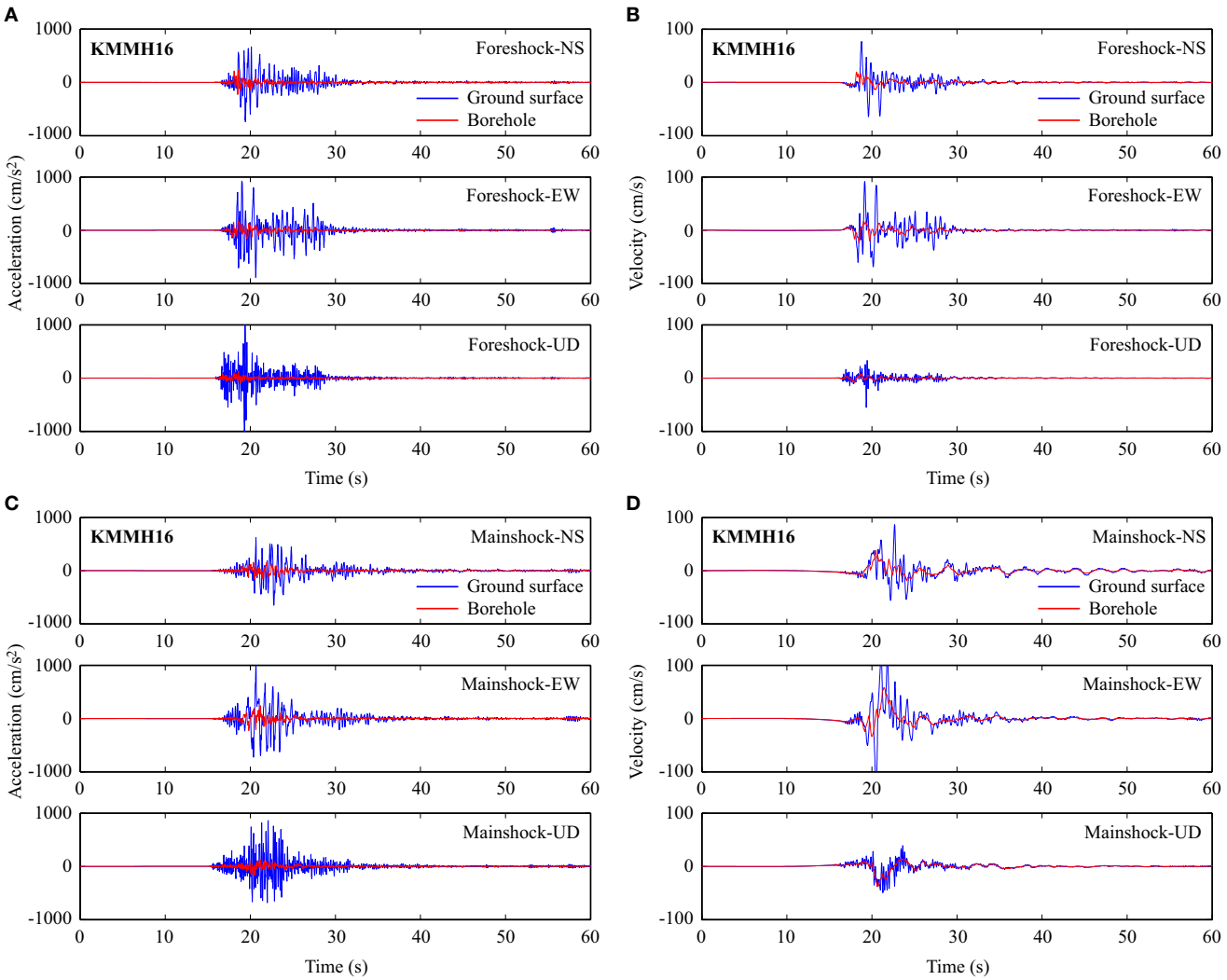

FIGURE 5 | **(A)** Acceleration time-histories for the foreshock at KMMH16. **(B)** Velocity time-histories for the foreshock at KMMH16. **(C)** Acceleration time-histories for the mainshock at KMMH16. **(D)** Velocity time-histories for the mainshock at KMMH16.

and KiK-net stations in the Kumamoto region, and for each station, two horizontal components on ground surface are rotated to a particular azimuth and then ground motion parameters are calculated using the rotated acceleration time-history. A rotation of ground motion records is carried out over 360° with 1° increment. The results can be plotted on a polar coordinate to examine the major and minor response axes of the ground motion records (Hong and Goda, 2007), in comparison with the fault orientation. The results for four ground motion parameters, i.e., PGA and SA at 0.3, 1.0, and 3.0 s, are shown in **Figure 8**; the response parameters in the EW and NS directions correspond to the responses due to un-rotated records. By focusing on the amplitudes of the responses (i.e., size of the response curve), **Figure 8** shows that intense ground motions due to the mainshock were observed over wide areas along the Futagawa and Hinagu faults. Large values of the ground motion parameters are particularly concentrated near KMMH16. Another notable feature of the results is the observation of intense ground shaking for SA at 3.0 s in the NE part of the map near KMM004 (**Figure 8D**).

Regarding the orientation of the major response axis of the observed ground motions, **Figure 8** shows that for PGA and SAs at 0.3 and 1.0 s, there is a clear dominant orientation of the ground motion parameters at KMMH16, KMM006, and KMM005, which is in parallel with the fault strike. Note that these stations are in the hanging wall region. Particularly for the short-period range, the trend of the major response orientation is consistent in the near-fault region. At longer vibration periods, the orientation of the major response axes at KMMH16 and KMM005 rotates to almost fault-normal direction, while that at KMM006 remains parallel with the fault strike. It is important to note that the major response directions at short-vibration periods for KMMH16 coincide with the directions of many collapsed houses in Mashiki Town. This indicates that in the near-fault region, effective countermeasures (e.g., bracing) can be implemented to mitigate shaking damage

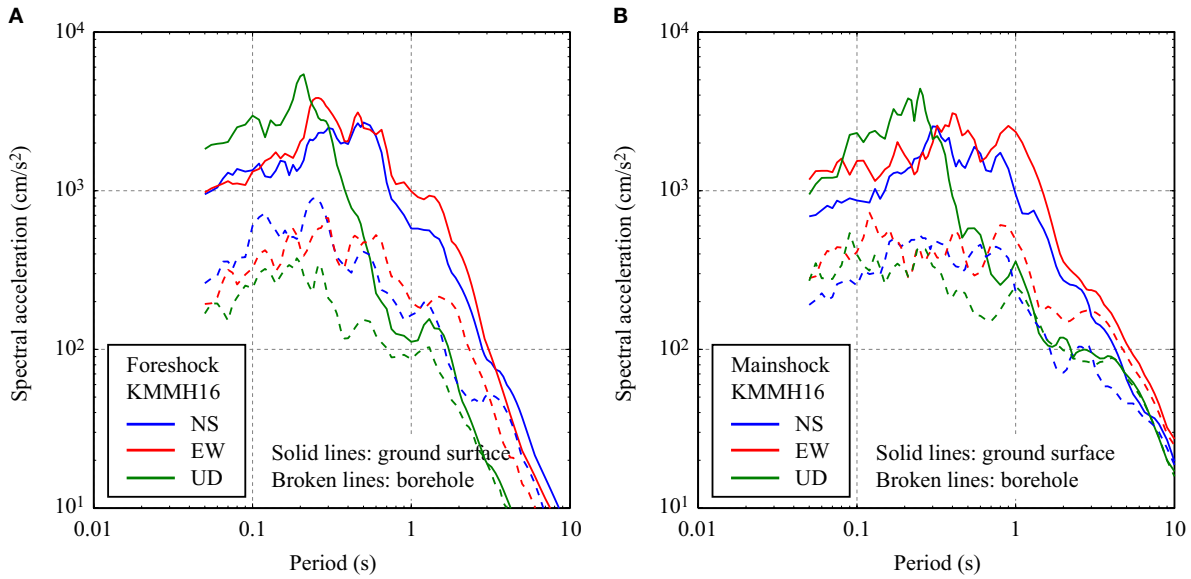

FIGURE 6 | **(A)** 5%-damped response spectra for the foreshock records at KMMH16. **(B)** 5%-damped response spectra for the mainshock records at KMMH16.

when the dominant direction of the ground shaking is known. Furthermore, outside the near-fault region, some consistent orientation effects can be observed. On the other hand, at KMM004, the fault-parallel component is dominant, particularly for SA at 3.0 s, noting that a large-amplitude velocity pulse is present in the EW component of the velocity time-history.

Comparison of Observed Ground Motions and Ground Motion Prediction Equations

It is important to compare the observed ground motions with existing empirical prediction models in the literature. Through such comparison, one can evaluate whether the ground motions from the Kumamoto earthquakes are unusual with respect to past events (note: such differences may arise due to various reasons, such as low/high stress drop and regional attenuation characteristics). In this study, a GMPE by Boore et al. (2014) is adopted. The Boore et al. model is developed using worldwide ground motion data for shallow crustal earthquakes (including ground motion data from Japanese earthquakes) and hence is well suited for such comparison. The moment magnitude for the mainshock is set to 7.1 according to F-net. The source-to-site distance for the Boore et al. model is based on the so-called Joyner-Boore distance; for the ground motion data from K-NET and KiK-net, this distance measure is evaluated using the GSI finite-fault plane geometry (**Figure 4A**). The Boore et al. model includes several adjustment parameters to refine the prediction, such as faulting mechanism and regional factor. In the comparison conducted herein, the strike-slip faulting mechanism and the regional factor for Japanese earthquakes are taken into account. For the comparison shown below, ground motion data that are recorded at sites with V_{s30} between 150 m/s and 500 m/s are considered (average V_{s30} is about 330 m/s). In applying the Boore et al. model, V_{s30} is set to 300 m/s. In the figures, to show the confidence interval of the Boore et al. model, curves that correspond to median plus/minus one SD are shown as broken lines, where the SD is the intra-event sigma as the predicted ground motions are compared with data from a single event.

Figure 9 compares observed ground motions with predicted mainshock ground motions, respectively, based on the Boore et al. model. The results for PGA and SAs at 0.3, 1.0, and 3.0 s are shown. The observed ground motions for the mainshock are generally consistent with the predicted values based on the Boore et al. model. In the distance range between 10 and 100 km, there are several observation data that exceed the median plus one sigma curve; these data are mainly located in the NE of the rupture zone (i.e., Yufu City and Kokonoe Town in Oita Prefecture). In these recorded accelerograms, the existence of a locally triggered event due to the mainshock was clearly observed; this increased the ground motion intensity at relatively remote locations. Overall, the recorded ground motion data for the mainshock of the Kuammoto sequence are in agreement with the Boore et al. prediction model (note: this conclusion is applicable to the majority of the earthquakes of the 2016 Kumamoto sequence).

Ground Motion Estimation at Unobserved Locations: Application to Kumamoto Port

The consistency of the observed ground motion data and the prediction model is useful for estimating ground motion parameters at unobserved locations where an estimate of experienced shaking intensity help understand the observed earthquake damage in the field. To improve the accuracy of ground motion estimation at unobserved locations, one can use both model predictions and observed ground motions nearby a site of interest by taking into account spatial correlation of ground motions (Goda and Hong, 2008; Bhattacharya and Goda, 2013). In this section, an application of the estimation

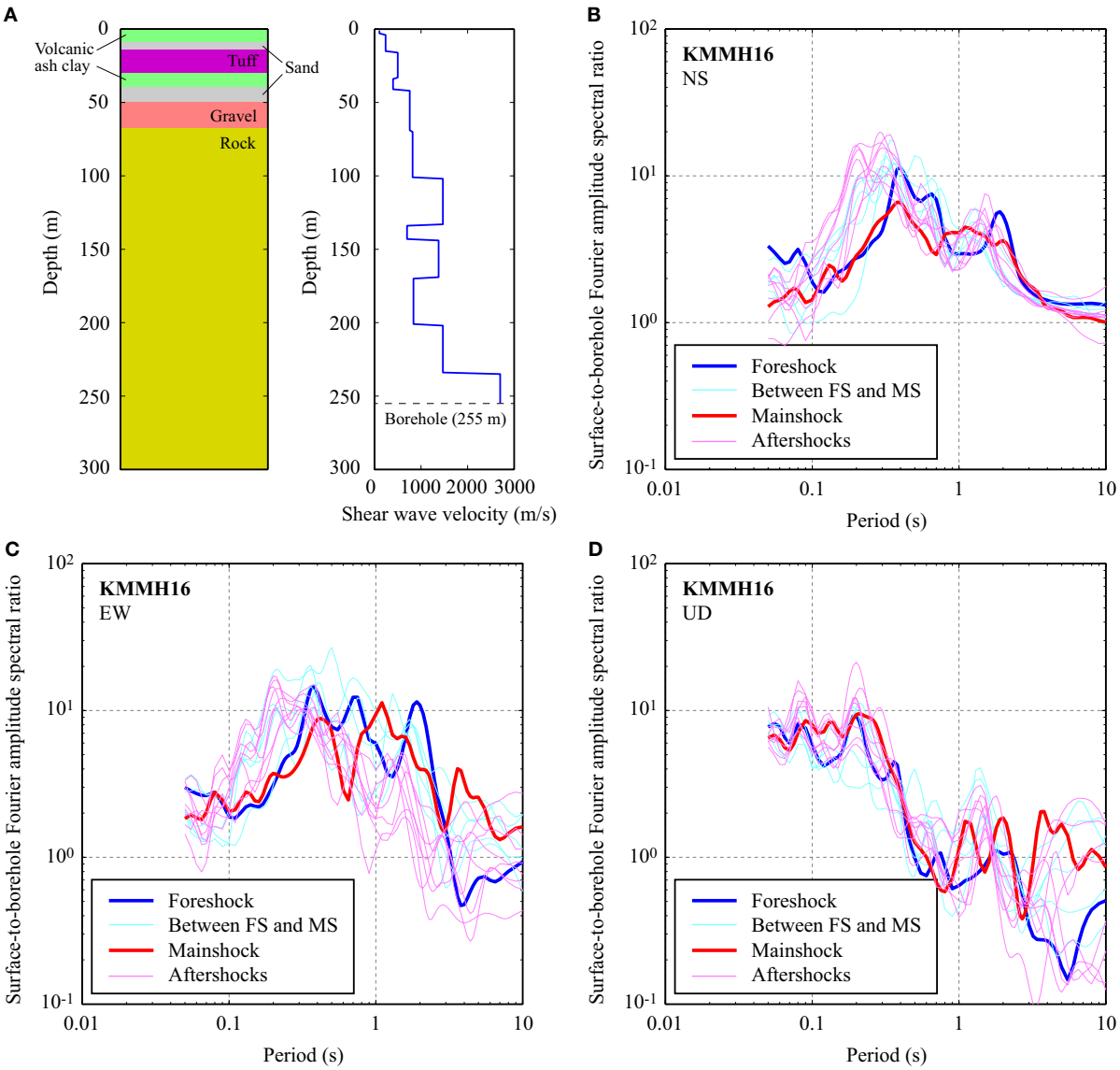

FIGURE 7 | **(A)** Borehole log and shear wave velocity profile at KMMH16. Surface-to-borehole ratios of Fourier amplitude spectra at KMMH16 for different earthquakes during the 2016 Kumamoto foreshock–mainshock–aftershock sequence: **(B)** NS components, **(C)** EW components, and **(D)** UD components.

method using a GMPE and spatial correlation model is demonstrated for Kumamoto port (32.7640°N, 130.5907°E), where liquefaction occurred during the Kumamoto mainshock but no actual recording of the ground motion was available. The nearest ground motion recording station is KMM008. The Joyner-Boore distance from the mainshock rupture plane to Kumamoto port is 15.0 km. The distance between Kumamoto port and KMM008 is 10.6 km.

For the estimation procedure outlined in Bhattacharya and Goda (2013), intra-event spatial correlation of ground motion residuals needs to be evaluated (Goda and Hong, 2008). The correlation model allows the interpolation of the observed ground motions at nearby recording stations to unobserved locations. The empirical spatial correlation curves for the Kumamoto mainshock ground motion data are shown in **Figure 10A**; each curve corresponds to a result for a ground motion parameter (e.g., PGA or SA at 0.3 s). The results show declining trends of the intra-event spatial correlation as a function of separation distance. The curves for different ground motion parameters vary. Overall, the spatial correlation coefficient of 0.5 is adopted as a representative value for the Kumamoto port and KMM008 (i.e., 10.6 km separation distance).

Using the observed response spectra at KMM008 (shown in **Figure 10B**), Boore et al. ground motion model, and spatial correlation coefficient (i.e., 0.5), response spectra at Kumamoto port are estimated. The average shear wave velocity at Kumamoto port is considered to be 200 m/s. The estimation results are shown in **Figure 10B**; both median and confidence

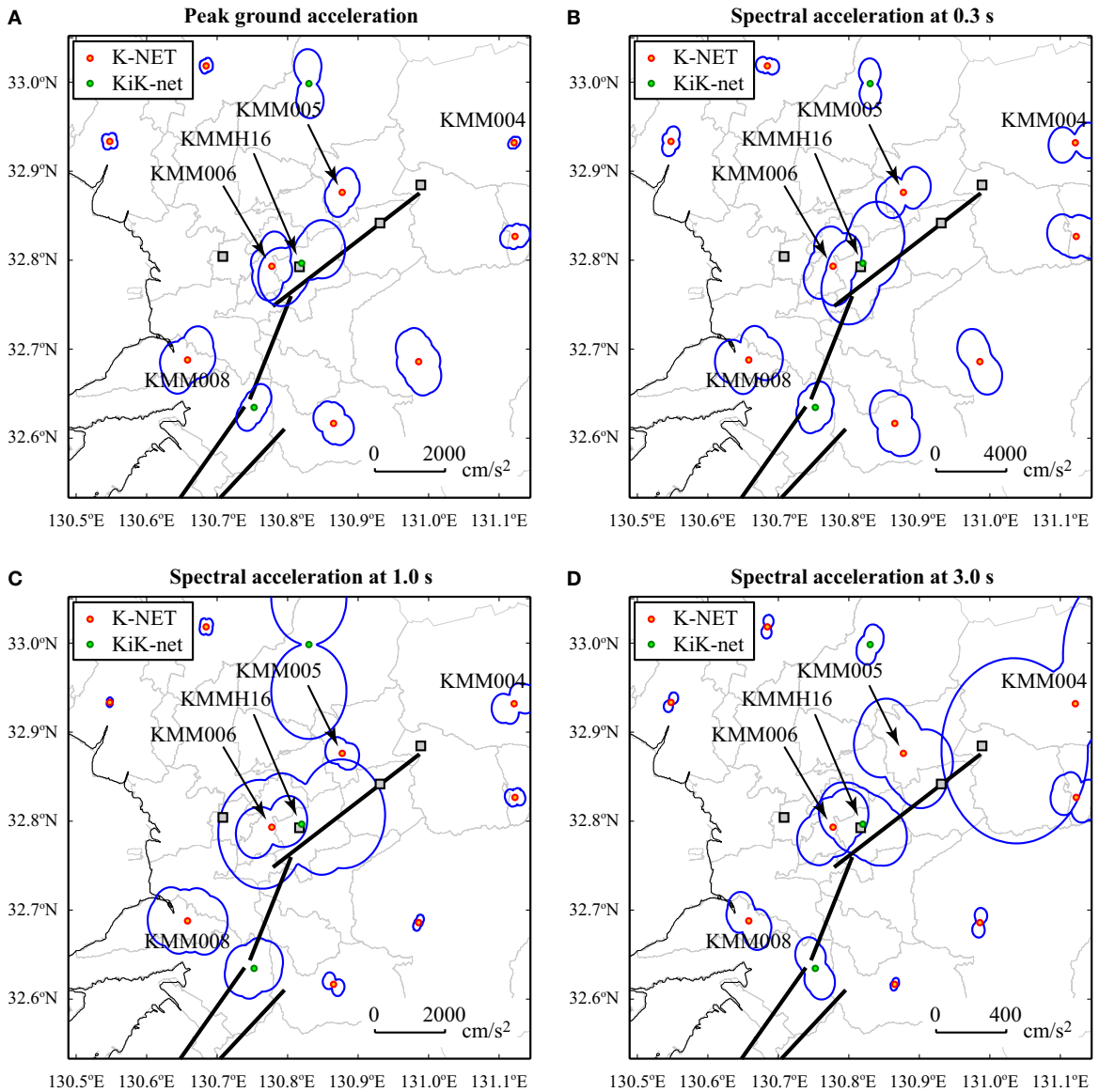

FIGURE 8 | **(A)** Acceleration time-histories for the mainshock at KMM006. **(B)** Velocity time-histories for the mainshock at KMM006. **(C)** Acceleration time-histories for the mainshock at KMM008. **(D)** Velocity time-histories for the mainshock at KMM008.

interval (16th and 84th percentiles) can be obtained through this method. For instance, the estimated PGA at Kumamoto port corresponds to a median of 0.48 g and a confidence interval ranges from 0.33 to 0.73 g (note: at KMM008, PGAs of 0.64 and 0.78 g were observed for the two horizontal components). The estimated PGA values are sufficiently large to trigger liquefaction for sandy soil layers (e.g., Idriss and Boulanger, 2008; Santucci de Magistris et al., 2013).

EARTHQUAKE DAMAGE SURVEYS

An earthquake damage investigation was conducted from May 22, 2016 to May 26, 2016. The main objective of the surveys was to assess the earthquake damage to buildings and infrastructure in relation to experienced fault rupture deformation and ground shaking. The surveyed sites include urban as well as rural areas of Kumamoto Prefecture. **Figure 11** shows three regions for the earthquake damage surveys; the locations of Regions 1, 2, and 3 are indicated in **Figure 1B**. Region 1 includes Kumamoto City and Uto City (i.e., urban areas in the Kumamoto plain); Region 2 includes Mashiki Town and Nishihara Village (i.e., rural areas outside of Aso Caldera), which are very close to the Futagawa fault and were shaken intensely during the mainshock; and Region 3 includes Minami Aso Village and Aso City, which are inside of Aso Caldera.

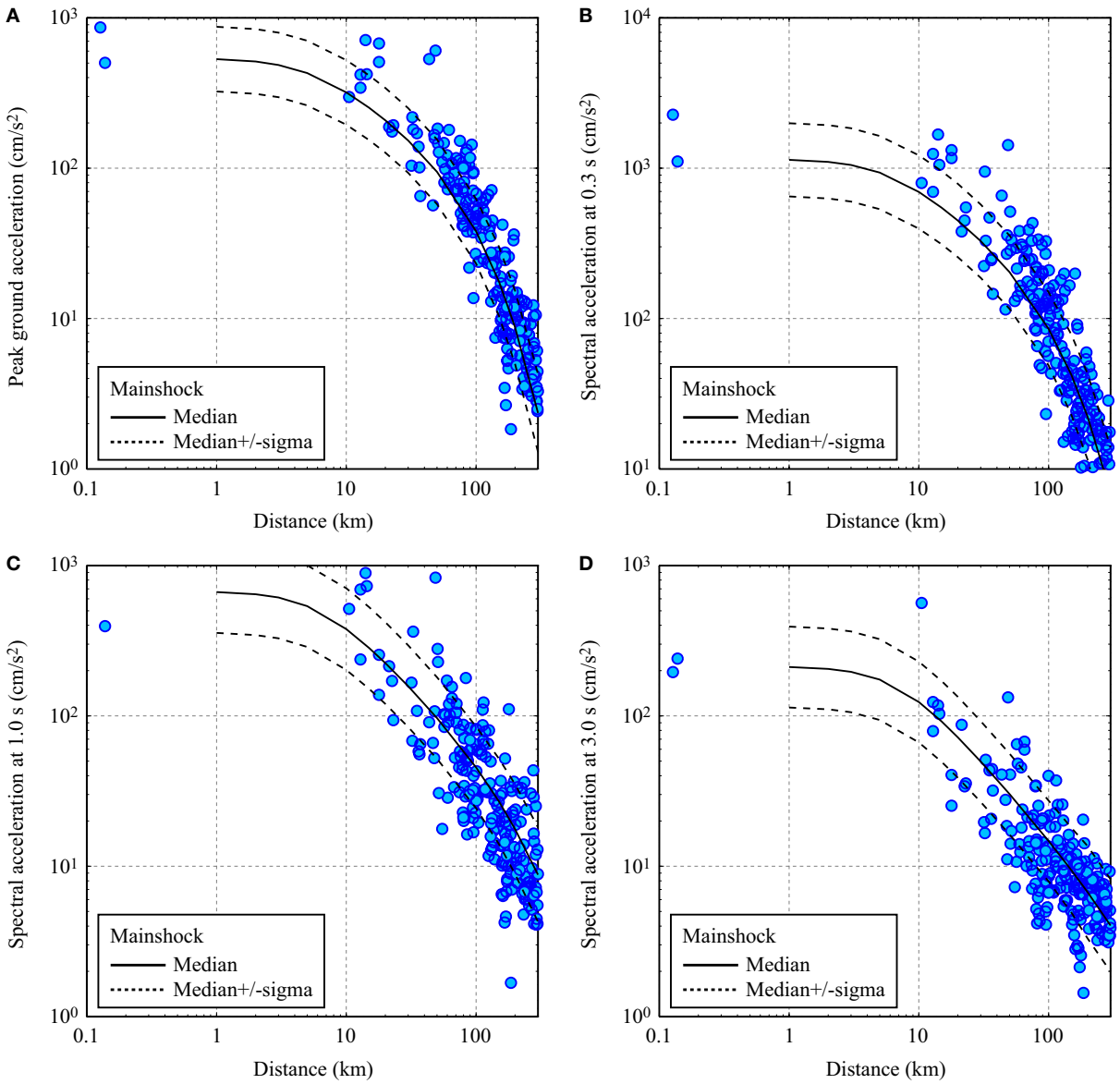

FIGURE 9 | Comparison of the observed ground motions with the prediction equation by Boore et al. (2014) for the mainshock: (A) peak ground acceleration, (B) spectral acceleration at 0.3 s, (C) spectral acceleration at 1.0 s, and (D) spectral acceleration at 3.0 s.

Damage in Kumamoto City and Uto City

A damage survey was conducted near Kumamoto Castle (i.e., downtown Kumamoto City; Location 1 in **Figure 11A**). A photo of Kumamoto Castle is shown in **Figure 12A**. The roof of the main castle (right-hand side) was damaged, and the wooden panels on the stone walls had collapsed. In fact, wooden panels as well as stone walls had collapsed at several places around the castle. At one location, the collapsed stone walls fell over a temple, destroying it. Along the moat of the castle, cracks were observed on the side walk and minor lateral spreading was observed (some buildings tilted toward the moat). During the walk-around survey in the downtown (near Kumamoto railway station and Kumamoto city office), damage to building cladding and external walls was observed (**Figure 12B**). Several high-rise buildings suffered earthquake damage, such as diagonal shear cracks that were visible from a distance. Although some old timber buildings suffered major damage and tilted (unrepairable damage), overall, major structural damage to modern buildings (timber/RC/steel) was neither major nor widespread, indicating that buildings in the city center performed well against the strong shaking experienced during the foreshock and mainshock.

Quick damage surveys were conducted near the KMM006 and KMM008 recording stations where actual recordings of

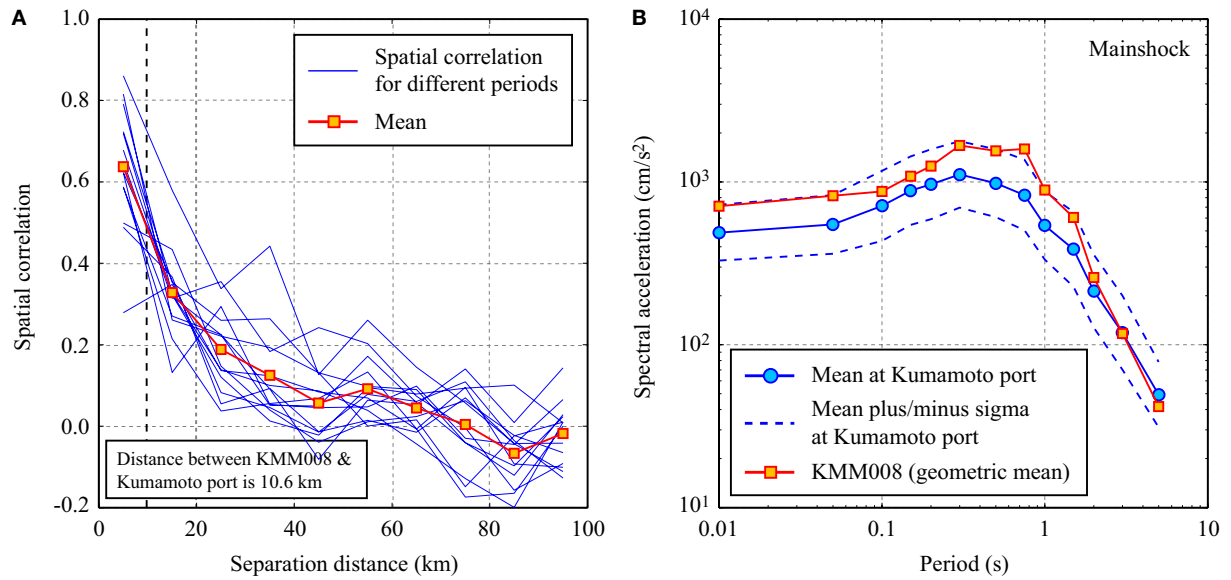

FIGURE 10 | **(A)** Spatial correlation of ground motion residuals for the mainshock. **(B)** Estimated response spectra at Kumamoto port based on the ground motion model by Boore et al. (2014) and the spatial correlation, conditioned on the observed ground motions at KMM008.

experienced ground motions were available. The KMM006 station was located in a residential area. The majority of houses in the neighborhood were two-story timber frames, and it appeared that they were constructed relatively recently. The buildings near KMM006 suffered slight damage only; the majority of the observed external damage was roof damage (**Figure 12C**). Near the KMM008 station (Location 2 in **Figure 11A**), no significant building damage was observed, except for the Uto city office, a 5-story reinforced concrete (RC) building (**Figure 12D**). The external RC frames of this city office suffered major damage, and the building was closed at the time of the survey. The third floor had partially collapsed, and window frames were distorted at the top two floors. Interestingly, the Uto city office was the only building in the area that was damaged significantly.

In the south of KMM006 (Location 3 in **Figure 11A**), a 9-story RC apartment was damaged (**Figure 12E**); many diagonal shear cracks were observed on walls at the lower three floors. Along Akitsu river (near Location 3 in **Figure 11A**), ground deformation and failures, including liquefaction, were reported. Moreover, a field investigation was conducted at Kumamoto port (Location 4 in **Figure 11A**). The port was constructed on a man-made island. Since the opening of Kumamoto port in 1993, the port has served as an important access route for people and goods. Some damage to port facilities was observed (e.g., overpass steel bridge at the ferry terminal). After the Kumamoto mainshock, sand boils were observed at the port as the sand used for reclamation was liquefiable (**Figure 12F**; note: borehole data at a site in the port island indicated a 3-m thick sand layer near the ground surface). The estimated ground motion at Kumamoto port, based on statistical analysis of observed ground motions at recording stations, indicates that the experienced PGA (typically 0.5 g) at Kumamoto port was sufficiently large to trigger liquefaction to landfilled sand layers.

Damage in Mashiki Town

Mashiki Town (location 5 in **Figure 11B**) was devastated by the 2016 Kumamoto earthquake sequence (both foreshock and mainshock). Numerous surface ruptures were observed in Mashiki Town (Shirahama et al., 2016). According to the seamless digital geological map of Japan[7], geological conditions near the Mashiki town office can be broadly categorized into two areas; geology of the northern part of Mashiki Town consists of deposits from pyroclastic flow of volcanic eruptions, while that of the southern part of Mashiki Town is formed by river terrace deposits.

Along Road 28, many buildings were severely damaged or had collapsed. The building shown in **Figure 13A** was a four-story steel building; the second floor had completely collapsed in a soft-story collapse mechanism. The majority of the buildings that had suffered a soft-story collapse had predominantly deformed/collapsed in the EW direction (more toward west), approximately parallel with Road 28 (e.g., **Figures 13A,B**). This coincides with the major response axes of the ground motion experienced in Mashiki Town (**Figure 8**). It has been reported that the effects due to the double-shock ground motions in Mashiki Town were significant. For example, a two-story steel building (**Figure 13B**) suffered minor-to-moderate damage due to the foreshock; however, it was destroyed by the subsequent mainshock. Several steel as well as RC buildings also suffered extensive damage. For instance, a RC-frame temple (**Figure 13C**) had collapsed due to the failures of beam-column joints (note: this building did not

[7]https://gbank.gsj.jp/seamless/index_en.html

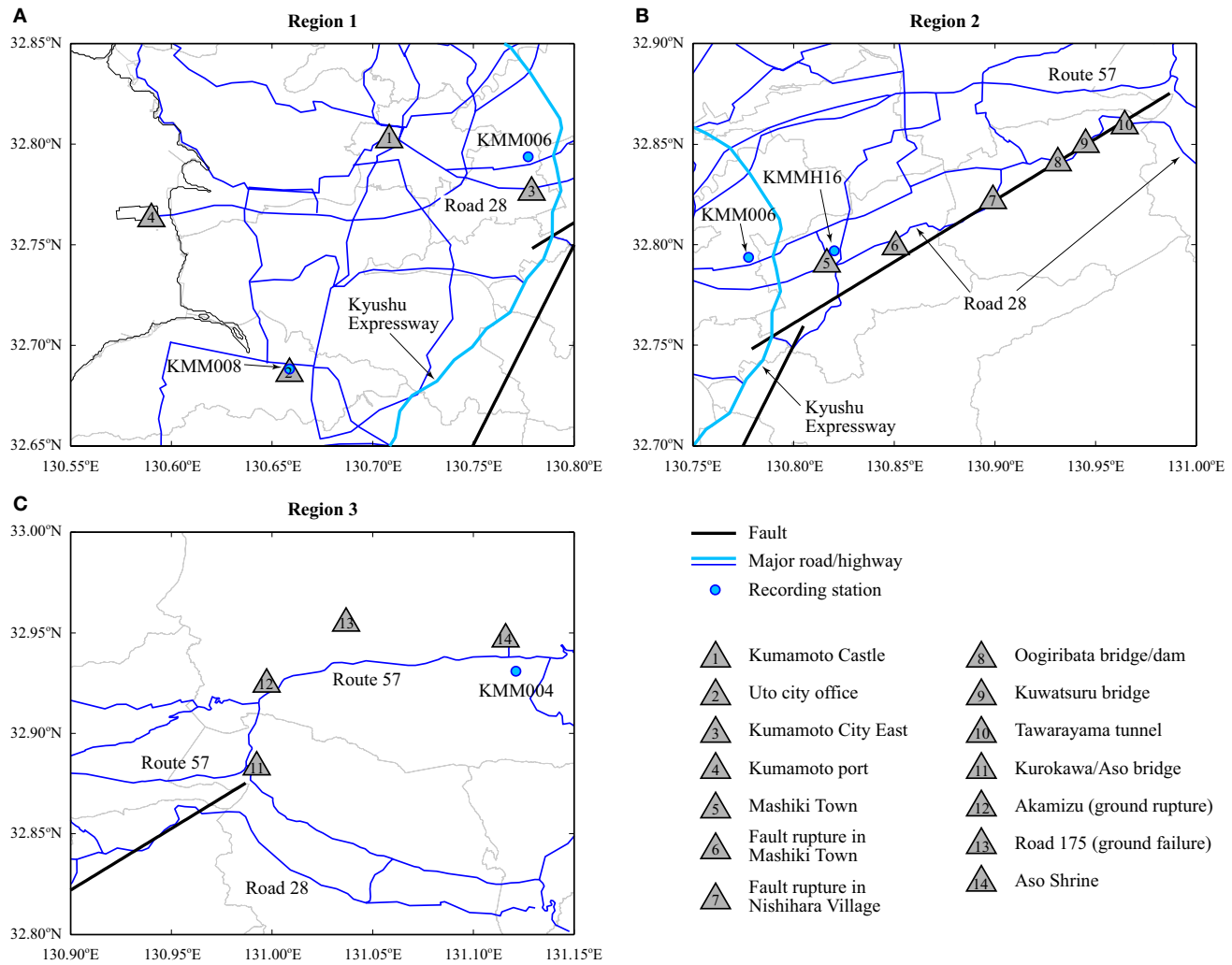

FIGURE 11 | **Locations of earthquake damage surveys: (A) region 1, (B) region 2, and (C) region 3**.

collapse after the foreshock but only suffered noticeable damage; it then collapsed due to the mainshock). Moreover, houses that were built on embankments suffered ground failures, and local soil conditions appear to be an important factor in the earthquake damage. For example, one row of six houses had collapsed partially due to foundation failures (**Figure 13D**). In the southern part of Mashiki Town (mainly agricultural areas along Kiyama river), uplifts of manholes were observed and settlements of the embankments along Kiyama river were seen (see also **Figure 15**), resulting in major gaps between the bridge deck and abutments. Typically, the bridge deck remained in its original position, while both sides of the embankments subsided by 0.4–0.5 m. RC piers of Daiichi Hatanaka bridge failed due to the ground deformation/failures (**Figure 13E**; Location 5 in **Figure 11B**; see also **Figure 15**). At the time of the survey, large sand bags (height of about 1 m) were placed along Kiyama river as temporary flood defenses. During the heavy rainfall on June 20 and 21, 2016 in Kumamoto, these temporary defenses were breached and Kiyama river and its surrounding areas were flooded. These are examples of the compounding disaster chain caused by the earthquakes and heavy rain.

The surface fault ruptures were observed in the paddy fields of Mashiki Town. **Figure 13F** shows the traces of the surface ruptures that appeared after the mainshock at Location 6 in **Figure 11B**. A clear misalignment of the ridge between paddy fields can be observed (circa 0.5–1.0 m, depending on the locations).

To understand the earthquake damage characteristics in Mashiki Town, a detailed damage survey was conducted near the Mashiki town office (note: JMA recording station was installed at the town office, which recorded the JMA intensity of 7 during the foreshock and mainshock). The surveyed areas were also close to the KMMH16 station. The surveys were carried out by two people to minimize the misassignment of the building damage grade. The survey was based on external visual inspections of buildings; building damage severity was assigned based on the

FIGURE 12 | **(A)** Damage to Kumamoto castle (location 1 in region 1). **(B)** Cladding damage to a building in the city center (location 1 in region 1). **(C)** Roof damage near KMM006. **(D)** Damage to the Uto city office (location 2 in region 1; near KMM008). **(E)** Damage to a high-rise residential building (location 3 in region 1). **(F)** Liquefaction site at Kumamoto port (location 4 in region 1).

earthquake damage grade categories that are similar to the EMS-98 guideline (Grünthal, 1998). Typically, five damage severities were considered: no damage, slight damage, moderate damage, heavy damage, and destruction. **Figure 14** shows examples of building damage classifications from the survey. During the survey, material type (wood, RC, steel, and unknown), story number, and use/occupancy class (residential, commercial, public, and etc.) were recorded in addition to the damage severity.

The results of the building damage survey in Mashiki Town are shown in **Figure 15**. In total, 277 buildings were inspected, consisting of 22 RC buildings, 15 steel buildings, 235 timber buildings, and 5 buildings with unknown material types. Out of 277 buildings, 47 buildings were undamaged, 63 buildings suffered slight damage, 50 buildings were heavily damaged, and 69 buildings were destroyed or are likely to be demolished due to unrepairable damage. Generally, newer timber houses as well as RC and steel buildings performed better than older timber houses. Houses in the south of the Mashiki town office were more severely damaged than those in the north, noting that the southern part of the surveyed areas was an older settlement. The differences of the damage extent in the northern and southern areas may also be attributed to geological conditions of the two areas (approximately, Road 28 is a boundary between the volcanic sediments and the river terrace deposits). Another important factor appeared to be the proximity to rivers (see **Figure 15**). Thus at the local scale, micro-zonation of soil types and geographical features may have been useful for evaluating seismic risk potential in this region *a priori*.

FIGURE 13 | **(A)** Collapsed steel building along Road 28 (location 5 in region 2). **(B)** Collapsed steel building along road 28 (location 5 in region 2). **(C)** Collapsed RC temple near the Mashiki town office (location 5 in region 2). **(D)** Building damage due to foundation failures (location 5 in region 2; near KMMH16). **(E)** Failures of RC piers of Daiichi Hatanaka bridge (location 5 in region 2). **(F)** Fault surface rupture (location 6 in region 2).

Damage in Nishihara Village

Nishihara Village is located outside of Aso Caldera and consists of a hilly/mountainous terrain. The eastern segment of the Futagawa fault traverses across Nishihara Village. EEFIT visited locations along the fault strike (**Figure 11B**), by following Road 28 (note: at several places Road 28 was blocked due to road failures and fallen objects). Along Road 28, many damaged/collapsed buildings (mainly timber houses) as well as landslides were observed. This section mainly focuses on infrastructure damage along Road 28 between Oogiribata bridge and Tawarayama tunnel. The Oogiribata-Tawarayama part of Road 28, an important access road to enter the Aso region, was not passable due to a series of bridge and road failures. It is noteworthy that the surveyed locations in Nishihara Village were very close to the Futagawa fault rupture zone, where large deformations and very intense ground shaking were observed. Therefore, it is likely that the causes of the observed infrastructure damage were due to the combined effects of the deformation and shaking.

A fault deformation and surface rupture in Nishihara Village were investigated at Location 7 in **Figure 11B**. The fault rupture cut across the ridge of a hill. At the surveyed location (a farmer's house and field), a vertical deformation up to 0.6 m was observed (**Figure 16A**). Buildings in the property suffered major damage or collapse; a timber structure (barn/storage) that was directly above

FIGURE 14 | Examples of damaged and collapsed timber buildings in Mashiki Town: (A) slight damage, (B) moderate damage, (C) heavy damage, and (D) collapse.

the fault rupture had collapsed, while the main house, a two-story timber building, was significantly damaged.

The major damage was observed near the Oogiribata reservoir (Location 8 in **Figure 11B**), which was essentially located directly above the Futagawa fault. The 23 m high earth-fill Oogiribata dam constructed in 1975 has been utilized for irrigation as well as fire-fighting purposes, and has played an important role in local communities. At the crest of Oogiribata dam, major surface rupture was observed (**Figure 16B**). The road pavements were destroyed due to compressional forces. The retaining walls of the spillway were damaged and were tilted significantly. Due to damage to the control gate for releasing water, a large volume of the stored water had leaked accidentally after the mainshock; no fatalities/casualties were reported to have been caused due to this damage.

In the same area, Oogiribata bridge, a curved 5-span steel girder bridge constructed in 2000, was damaged significantly. The bridge was constructed to bypass a valley, where a major landslide occurred along the slope; the slipped soils might have affected the bridge piers at their base. Large cracks and gaps were observed at both sides of the abutments/roads. At the upper side of the bridge, all five bridge supports, i.e., laminated rubber bearing, had sheared/ruptured completely (**Figure 16C**). Consequently, the bridge deck was dismantled and displaced by about 0.3–0.4 m toward the valley side of the slope (**Figure 16D**).

Along Road 28 to Tawarayama tunnel, which is about 2 km long and connects Nishihara Village and Minami Aso Village (i.e., outside and inside of Aso Caldera), major damage to bridges and roads was caused. For instance, Kuwatsuru bridge, a cable-stayed bridge constructed in 1997, was damaged severely due to significant settlements of bridge abutments, resulting in a gap of 0.3–0.4 m (**Figure 16E**). At Tawarayama bridge near the tunnel, similar abutment/ground failures were observed. In addition, several landslides/slope failures were observed along Road 28; some of them caused major damage to roads (**Figure 16F**). Tawarayama tunnel was also damaged due to the mainshock and was not passable at the time of the survey. Large cracks were observed on the concrete cover near the entrance of the tunnel (**Figure 16G**).

Damage in Minami Aso Village and Aso City

Minami Aso Village, which lies between Aso Mountains and Aso Caldera, was devastated by the Kumamoto mainshock. The earthquake damage in the Kurokawa district of Minami Aso Village (Location 11 in **Figure 11C**) was significant. Many timber buildings were destroyed (**Figure 17A**), and the surface ruptures were also observed. In the Kurokawa district, a detailed damage survey was carried out; the survey was led by the Kyoto

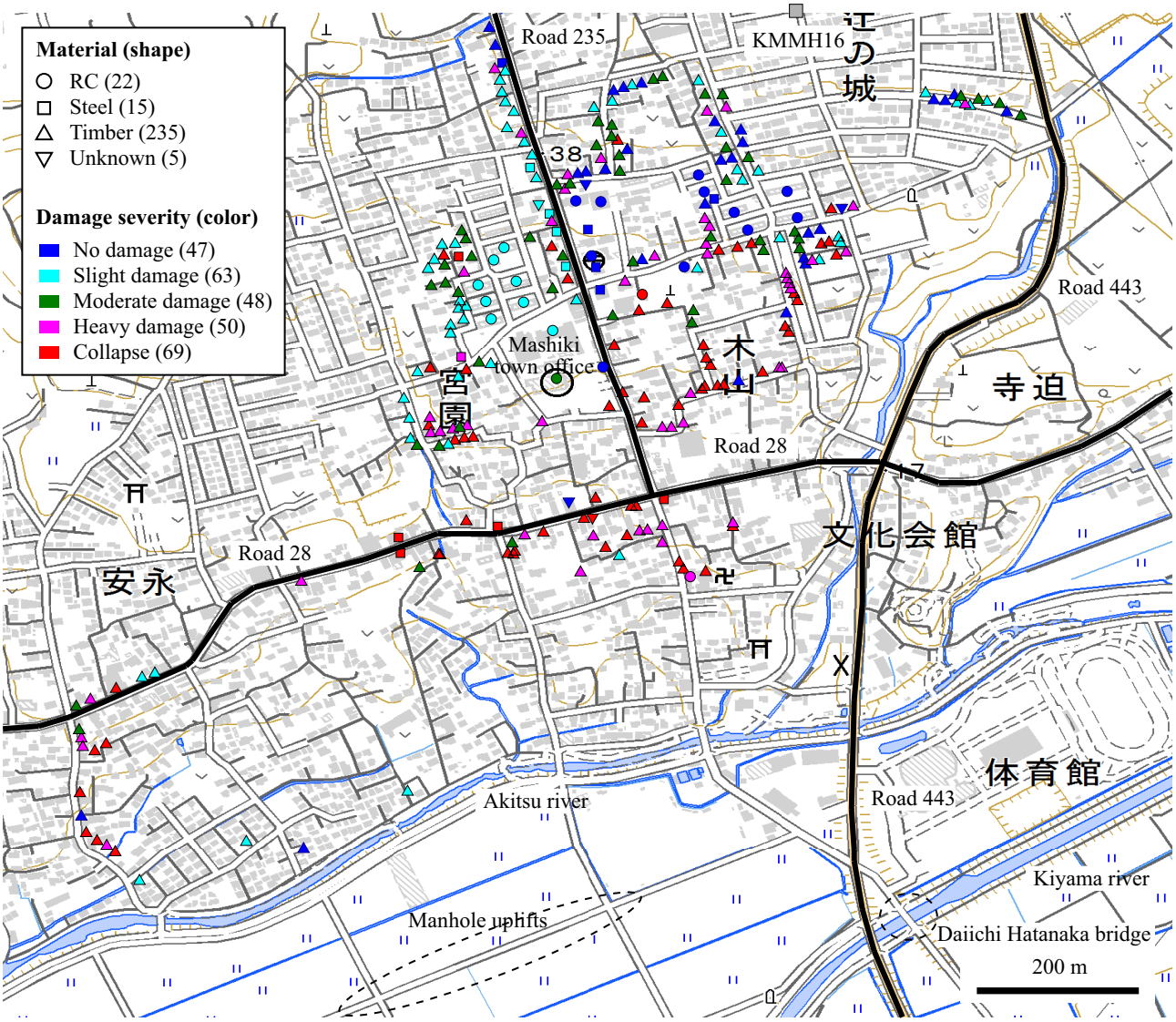

FIGURE 15 | **Damage survey results in Mashiki Town**. The base map was obtained from the Geospatial Institute of Japan.

University group. The results are presented in **Figure 18** (the format is similar to those shown in **Figure 15** for Mashiki Town). In total, 138 buildings were inspected; the majority of the surveyed structures were residential timber houses, while RC buildings were an elementary school and apartment buildings. **Figure 18** shows that more than a half of the timber houses had collapsed due to the mainshock. On the other hand, larger RC structures were not damaged. To examine the correlation between observed surface ruptures and building damage, videos taken from a UAV (unmanned aerial vehicle) that were provided by the GSI were analyzed. The identified surface ruptures in the Kurokawa district are indicated in **Figure 18**. It can be observed that some of the surface ruptures cut underneath buildings, which were destroyed.

One of the most significant events during the Kumamoto earthquake was the large-scale landslide in the Tateno district (**Figure 17B**; approximately, 700 m long and 200 m wide), which destroyed Route 57, which connected Kumamoto Prefecture and Oita Prefecture *via* Aso Caldera. The landslide caused the collapse of Aso bridge (Location 11 in **Figure 11C**). Aso bridge was a steel reversed Langer bridge constructed in 1970 crossing over Kurokawa river, and was a part of the regional road network, connecting the Tateno district and the Kurokawa district of Minami Aso Village (i.e., outside and inside of Aso Caldera). It is important to recognize that the Futagawa fault cut underneath of Aso bridge; henceforth, differential ground deformations at both sides of the bridge could have been significant (because of the strike-slip faulting and the locations are very near to the fault strike; see **Figure 4**). The collapse of Aso bridge may be due to the combined effects of the ground deformation and the landslide. More investigations are warranted regarding the exact cause of the bridge collapse.

FIGURE 16 | **(A)** Fault surface rupture in Mashiki Town (location 7 in region 2). **(B)** Fault surface rupture at the crest of Oogiribata dam (location 8 in region 2). **(C)** Shear fracture of bridge support underneath Oogiribata bridge (location 8 in region 2). **(D)** Damage to Oogiribata bridge (location 8 in region 2). **(E)** Damage to Kuwatsuru bridge (location 9 in region 2). **(F)** Road failure near Tawarayama tunnel (location 10 in region 2). **(G)** Cracks inside Tawarayama tunnel (location 10 in region 2).

Near Aso bridge, several other bridges that served as alternative access route between Minami Aso Village and Kumamoto downtown, were also damaged and made unpassable due to the mainshock. **Figure 17C** shows Choyo bridge, located in the Tateno district (downstream of Aso bridge along Kurokawa river); the abutment of the bridge had subsided significantly (even visible in **Figure 17C**).

Overall, simultaneous destruction of the access routes that connected areas inside and outside of Aso Caldera, i.e., Oogiribata-Tawarayama route (Road 28), Kumamoto-Oita route (Route 57), Tateno-Kurokawa route (Aso bridge), Tateno-Choyo route (Choyo bridge), caused significant disruptions and delays in rescue and evacuation operations immediately after the mainshock. At the time of the survey, major detours were necessary. This demonstrates the critical importance of the disaster recovery process in ensuring community resilience. The repairs and reconstructions of the key infrastructure in the near-fault region are important aspects of the overall seismic resilience and community resilience and need to be considered from a holistic perspective.

The earthquake damage surveys were also carried out in Aso City, NE of the fault rupture zone. Near the Akamizu railway station (Location 12 in **Figure 11C**), ground failures were observed in the paddy field (**Figure 17D**); about 0.7 m

FIGURE 17 | **(A)** Collapsed timber building in the Kurokawa district of Minami Aso Village (Location 11 in Region 3). **(B)** Route 57 blockage due to the landslide near Aso bridge (location 11 in Region 3). **(C)** Damage to Choyo bridge (location 11 in Region 3). **(D)** Ground cracks near the Akamizu railway station (location 12 in region 3). **(E)** Ground settlement over a timber house (location 13 in region 3). **(F)** Collapse of Aso Shrine (location 14 in region 3).

subsidence of the ground was observed. The direct cause of the subsidence is not yet known because the location is relatively distant from the fault rupture zone. Similar ground settlements were observed along Road 175 (Location 13 in **Figure 11C**). Subsidence of about 1.0–1.5 m was observed, depending on the locations. Houses directly above the ground cracks had been destroyed (**Figure 17E**), while houses on the subsided portion of the ground were intact (no viable damage externally). These ground failures were localized.

Earthquake Engineering Field Investigation Team also visited Aso Shrine (Location 14 in **Figure 11C**), which is designated as important cultural properties of the nation. The main structures of Aso Shrine had been destroyed by the mainshock (**Figure 17F**). On the other hand, in the surrounding areas of Aso Shrine, no obvious ground failures were observed. Because large long-period ground motions were recorded at the KMM004 station (**Figure 8**) and roof structures were heavy, the main cause of the collapse of Aso Shrine may be attributed to the shaking. Nonetheless, more investigations are warranted to understand the exact cause of the exceptionally large ground motions in these areas, which are remote from the fault rupture zone.

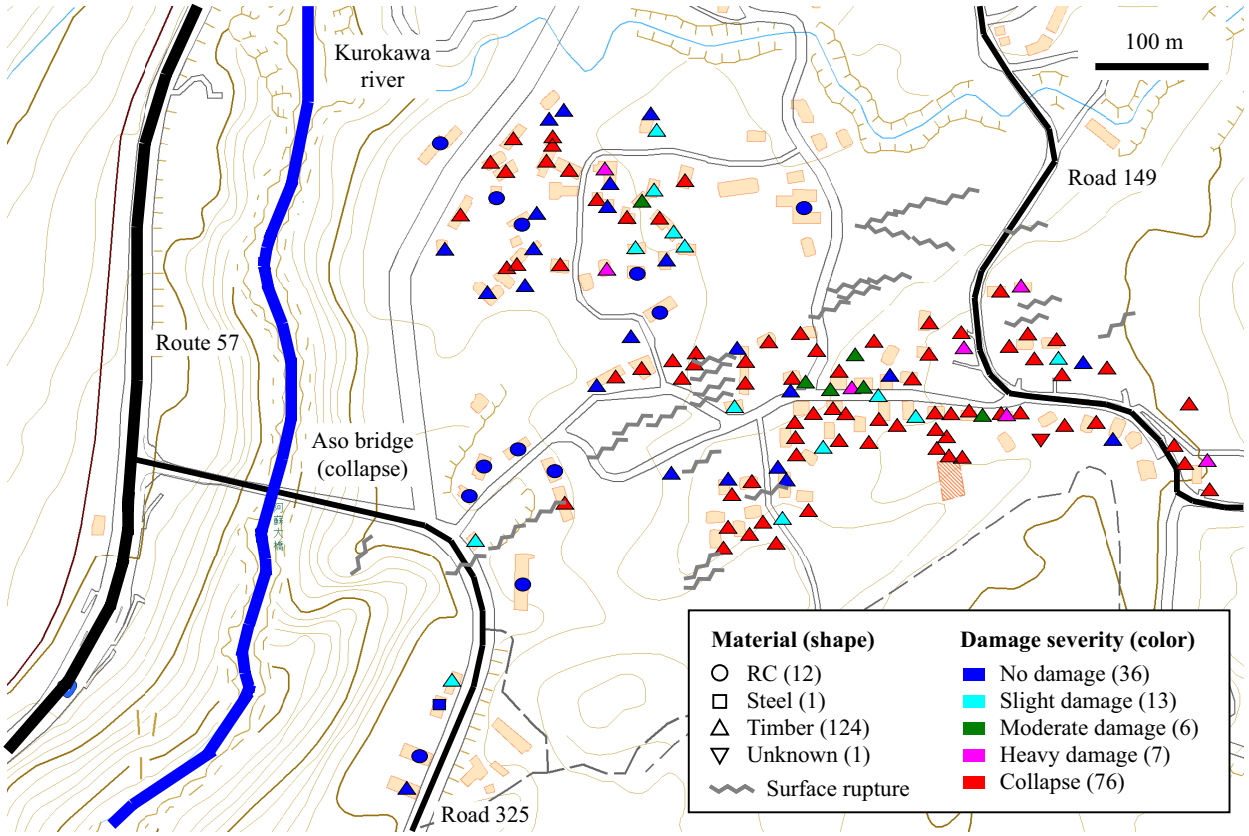

FIGURE 18 | Damage survey results in the Kurokawa district of Minami Aso village. The base map was obtained from the Geospatial Institute of Japan.

SUMMARY AND CONCLUSIONS

The 2016 Kumamoto earthquake sequence, consisting of an M_J 6.5 foreshock, an M_J 7.3 mainshock, and numerous aftershocks, caused significant damage to buildings and infrastructure in the intraplate region of Kyushu Island, Japan, apart from subduction zones. The earthquakes occurred along the Hinagu–Futagawa fault zones, which were considered to be capable of hosting M_w 7 earthquakes based on geological investigations but have not been particularly active in recent history. Consequently, the occurrence of the 2016 Kumamoto earthquakes was perceived as a surprise. The building stock in the Kumamoto region was not particularly resistant to intense ground shaking, resulting in the destruction and damage of more than 8,000 houses and 120,000 houses, respectively (as of 1 July 2016). Furthermore, significant effects due to large ground deformation were observed, and bridges and roads in the near-fault zone were damaged severely. On the other hand, during the earthquake sequence, numerous recordings of geophysical data, such as GPS measurements and strong motion time-histories, were obtained. These data are valuable in reconstructing the rupture processes of the earthquakes *via* rigorous inversion analysis. In addition, many field and remote sensing data (e.g., building damage surveys, fault rupture measurements, landslide occurrence, and ground deformation based on InSAR imagery) were collected and these are particularly useful for gaining deeper understanding of the main causes of the earthquake damage.

To learn key lessons from the observed damage and impact due to the Kumamoto earthquakes, a field investigation team was dispatched from the UK, and conducted earthquake damage reconnaissance surveys in Kumamoto. As part of the investigations, regional earthquake catalog data and strong motion data were analyzed. In particular, the ground deformation profiles were evaluated based on available finite-fault models for the Kumamoto earthquakes, and were compared with actual GPS measurements before and after the earthquakes. Detailed analyses of recorded ground motions in the near-fault zone (e.g., KMMH16) revealed striking features of the intense ground shaking, directivity of strong motion, and site amplification. The analyzed data were compared with an existing ground motion model for shallow crustal earthquakes. The earthquake damage surveys focused on locations near the fault rupture zone of the mainshock, i.e., Mashiki Town, Nishihara Village, and Minami Aso Village. Moreover, detailed damage surveys were conducted in Mashiki Town and Minami Aso Village to investigate the key contributing factors in the earthquake damage. The investigations of infrastructure damage in the near-fault zone showed significant impact due to substantial ground deformation.

The main results from the earthquake data analyses for the Kumamoto events are as follows:

1. Seismic activities of the 2016 Kumamoto sequence were distributed over a wide region, triggering numerous aftershocks. The migration of the earthquakes, originally from the Hinagu fault zone (i.e., foreshock) to the Futagawa fault zone (i.e., mainshock), was a notable feature of the sequence.
2. The recorded ground motions in the hanging wall region (e.g., KMMH16 in Mashiki Town) showed intense spectral acceleration amplitudes in the short-to-moderate vibration period range (exceeding 1 g) with significant site amplification due to soft sediments in the Kumamoto plain.
3. A clear directivity of ground motions in parallel with the fault strike was observed in the near-fault zone, which correlated well with the fallen directions of collapsed buildings in Mashiki Town.
4. The observed ground motion data were in agreement with an empirical ground motion model by Boore et al. (2014). Furthermore, typical decaying behavior for spatial correlation of the ground motion residuals was obtained as a function of inter-station distance. These results are useful for estimating ground motion parameters at unobserved locations. An application of the advanced ground motion estimation technique was demonstrated for a liquefaction site at Kumamoto port.

The main results from the earthquake damage surveys in the Kumamoto region are summarized as follows:

5. The earthquake damage in the Kumamoto downtown was relatively minor, despite the intense ground shaking experienced; however, major damage to Kumamoto Castle was caused. As locations become closer to the fault rupture zone, the occurrence of the structural damage become more frequent.
6. The building damage in Mashiki Town was extensive; numerous building collapses were observed. Influential factors of the earthquake damage occurrence include the construction material (timber versus steel/RC), construction age (old versus modern constructions), geological/geographical condition (e.g., proximity to rivers). In the near-fault region, the effects of ground deformation were also significant (e.g., settlement and slope failures). A detailed micro-zonation study would be useful for assessing the seismic risk potential of existing building stock.
7. More than 50% of the timber houses in the Kurokawa district of Minami Aso Village were destroyed by the mainshock; the causes of the building collapse were attributed to both strong ground shaking and surface ruptures.
8. The ground deformation and shaking in the near-fault zone affected various kinds of infrastructure, such as bridges, roads, and tunnels. During the mainshock, failures of the infrastructure occurred simultaneously at many locations, essentially disconnecting existing access routes between cities and towns inside Aso Caldera and those outside. Significant disruptions and delays in rescue and evacuation operations were caused due to destruction of the regional traffic network. The issues of maintaining the essential functionality of infrastructure are critical for communities that may be isolated after the major earthquake.

During and after the earthquakes, numerous incidents of compounded disasters were observed. For instance, a heavy rainfall in the Kumamoto region has led to occurrence of additional landslides, debris flows, and flooding. In the recovery process, viable solutions should be sought for by taking a holistic viewpoint of disaster resilience and sustainability of communities.

AUTHOR CONTRIBUTIONS

All authors contributed to the preparation of the submitted manuscript.

ACKNOWLEDGMENTS

The work is funded by the EPSRC grant (EP/I01778X/1) for the Earthquake Engineering Field Investigation Team (EEFIT). The financial supports for industrial members (GC, LH, LK, and RM) are provided by Arup, Mott MacDonald, and Willis. The first author is grateful to Dr. Takashi Kiyota, who generously shared his earthquake damage survey results immediately after the earthquake. The survey results by Dr. Kiyota can be found in http://www.gdm.iis.u-tokyo.ac.jp/index_e.html. The EEFIT members thank Prof Shinji Toda and Ms Zoe Mildon for sharing the information on the surface rupture locations. The JMA catalog was obtained from http://www.hinet.bosai.go.jp/, and ground motion data were obtained from http://www.kyoshin.bosai.go.jp/. The elevation data were obtained from https://asterweb.jpl.nasa.gov/gdem.asp.

SUPPLEMENTARY MATERIAL

The Supplementary Material for this article can be found online at http://journal.frontiersin.org/article/10.3389/fbuil.2016.00019

The collected earthquake damage data (i.e., geocoded pictures) of the 2016 Kumamoto EEFIT mission can be obtained from the supplementary information accompanying this paper (i.e., Google Earth kmz file).

REFERENCES

Bhattacharya, S., and Goda, K. (2013). Probabilistic buckling analysis of axially loaded piles in liquefiable soils. *Soil Dyn. Earthq. Eng.* 45, 13–24. doi:10.1016/j.soildyn.2012.10.004

Boore, D. M. (2005). On pads and filters: processing strong-motion data. *Bull. Seismol. Soc. Am.* 95, 745–750. doi:10.1785/0120040160

Boore, D. M., Stewart, J. P., Seyhan, E., and Atkinson, G. M. (2014). NGA-West 2 equations for predicting PGA, PGV, and 5%-damped PSA for shallow crustal earthquakes. *Earthq. Spectra* 30, 1057–1085. doi:10.1193/070113EQS184M

Cabinet Office of Government of Japan. (2016). *Estimated Economic Impact Due to the 2016 Kumamoto Earthquakes*. Available at: http://www5.cao.go.jp/keizai3/kumamotoshisan/kumamotoshisan20160523.pdf [accessed June 9, 2016].

Fire and Disaster Management Agency (2016). Available at http://www.fdma.go.jp/bn/2016/

Fraser, S., Pomonis, A., Raby, A., Goda, K., Chian, S. C., Macabuag, J., et al. (2013). Tsunami damage to coastal defences and buildings in the March 11th 2011 M_w9.0 Great East Japan earthquake and tsunami. *Bull. Earthq. Eng.* 11, 205–239. doi:10.1007/s10518-012-9348-9

General Insurance Association of Japan. (2016). *Key Figures Related to Insurance Claims Due to the 2016 Kumamoto Earthquake as of June 13, 2016*. Available at: http://www.sonpo.or.jp/en/news/2016/1606_03.html [accessed June 18, 2016].

Geospatial Institute of Japan (GSI). (2016). *The 2016 Kumamoto Earthquake*. Available at: http://www.gsi.go.jp/BOUSAI/H27-kumamoto-earthquake-index.html [accessed June 18, 2016].

Ghofrani, H., Atkinson, G. M., and Goda, K. (2013). Implications of the 2011 M9.0 Tohoku Japan earthquake for the treatment of site effects in large earthquakes. *Bull. Earthq. Eng.* 11, 171–203. doi:10.1007/s10518-012-9413-4

Goda, K., and Hong, H. P. (2008). Spatial correlation of peak ground motions and response spectra. *Bull. Seismol. Soc. Am.* 98, 354–365. doi:10.1785/0120070078

Goda, K., Pomonis, A., Chian, S. C., Offord, M., Saito, K., Sammonds, P., et al. (2013). Ground motion characteristics and shaking damage of the 11th March 2011 M_w9.0 Great East Japan earthquake. *Bull. Earthq. Eng.* 11, 141–170. doi:10.1007/s10518-012-9371-x

Grünthal, G. (1998). *European Macroseismic Scale 1998 (EMS-98)*. Luxembourg: Centre Européen de Géodynamique et de Séismologie, 99.

Guo, Z., and Ogata, Y. (1997). Statistical relations between the parameters of aftershocks in time, space, and magnitude. *J. Geophys. Res.* 102, 2857–2873. doi:10.1029/96JB02946

Headquarters for Earthquake Research Promotion. (2016). *Evaluation of the Futagawa and Hinagu Fault Zones*. Available at: http://www.jishin.go.jp/main/chousa/13feb_chi_kyushu/k_11.pdf [accessed May 15, 2016].

Hong, H. P., and Goda, K. (2007). Orientation-dependent ground motion measure for seismic hazard assessment. *Bull. Seismol. Soc. Am.* 97, 1525–1538. doi:10.1785/0120060194

Idriss, I. M., and Boulanger, R. W. (2008). *Soil Liquefaction During Earthquakes*. Oakland, CA: Earthquake Engineering Research Institute.

Irikura, K., and Miyake, H. (2011). Recipe for predicting strong ground motion from crustal earthquake scenarios. *Pure Appl. Geophys.* 164, 85–104. doi:10.1007/s00024-010-0150-9

Kojima, K., and Takewaki, I. (2016). A simple evaluation method of seismic resistance of residential house under two consecutive severe ground motions with intensity 7. *Front. Built Environ.* 2:15. doi:10.3389/fbuil.2016.00015

Nakashima, M., and Chusilp, P. (2003). A partial view of Japanese post-Kobe seismic design and construction practices. *Earthq. Eng. Eng. Seismol.* 4, 3–13.

National Institute of Advanced Industrial Science and Technology. (2016). *Active Fault Database of Japan*. Available at: https://gbank.gsj.jp/activefault/index_e_gmap.html [accessed June 7, 2016].

Okada, Y. (1985). Surface deformation due to shear and tensile faults in a half-space. *Bull. Seismol. Soc. Am.* 75, 1135–1154.

Okumura, K. (2016). *Earthquake Geology of the April 14 and 16, 2016 Kumamoto Earthquakes*. Available at: http://home.hiroshima-u.ac.jp/kojiok/kumamoto2016KOreport2.pdf [accessed May 15, 2016].

Santucci de Magistris, F., Lanzano, G., Forte, G., and Fabbrocino, G. (2013). A database for PGA threshold in liquefaction occurrence. *Soil Dyn. Earthq. Eng.* 54, 17–19. doi:10.1016/j.soildyn.2013.07.011

Sawazaki, K., Sato, H., Nakahara, H., and Nishimura, T. (2009). Time-lapse changes of seismic velocity in the shallow ground caused by strong ground motion shock of the 2000 Western-Tottori earthquake, Japan, as revealed from coda deconvolution analysis. *Bull. Seismol. Soc. Am.* 99, 352–366. doi:10.1785/0120080058

Shirahama, Y., Mori, H., Maruyama, T., and Yoshimi, M. (2016). *Geological Survey of Japan AIST Emergency Survey Report*. Available at: http://g-ever.org/updates/?p=334 [accessed June 7, 2016].

Watson-Lamprey, J., and Boore, D. M. (2007). Beyond $S_{aGMRotI}$: conversion to S_{aArb}, S_{aSN} and $S_{aMaxRot}$. *Bull. Seismol. Soc. Am.* 97, 1511–1524. doi:10.1785/0120070007

Wu, C., Peng, Z., and Assimaki, D. (2009). Temporal changes in site response associated with strong ground motion of 2004 M6.6 mid-Niigata earthquake sequences in Japan. *Bull. Seismol. Soc. Am.* 99, 3487–3495. doi:10.1785/0120090108

Conflict of Interest Statement: The authors declare that the research was conducted in the absence of any commercial or financial relationships that could be construed as a potential conflict of interest.